Optimal monitoring design for uncertainty quantification during geologic CO_2 sequestration: A machine learning approach

Misael M. Morales[a,b,*], **Mohamed Mehana**[a,*] **Bailian Chen**[a],

(a) Earth and Environmental Sciences Division, Los Alamos National Laboratory

(b) Hildebrand Department of Petroleum and Geosystems Engineering, The University of Texas at Austin

*Corresponding author; email: misaelmorales@lanl.gov, mzm@lanl.gov

Highlights

Filtering-based data assimilation method is developed to perform monitoring design.

Machine learning reduced-order model is used to reduce computational cost of data assimilation process.

Monitoring well placement optimization is performed to reduce uncertainty and minimize leakage risks.

Keywords

Geologic carbon sequestration; Monitoring design optimization; Machine Learning; Reduced-order modeling; Data assimilation; Uncertainty quantification

Abstract

Geologic CO_2 sequestration (GCS) projects have large uncertainties in geologic properties, and require optimal monitoring designs for risk assessment and management. An effective monitoring design is crucial to ensure the safe and permanent geologic storage of CO_2. Optimal monitoring design involve an optimal placement of monitoring wells, and optimal monitoring measurement data (pressure, CO_2 saturation, temperature, etc.). We have developed a filtering-based data assimilation approach to design an optimal GCS monitoring strategy for well placement and monitoring data design. To efficiently solve the optimization problem and reduce computational costs, Artificial Neural Networks are used to develop computationally efficient reduced-order models based on full-physics numerical simulations of CO_2 injection in saline aquifers. We demonstrate our approach in two scenarios of CO_2 leakage through legacy or abandoned wellbores where an optimal monitoring strategy are devised to reduce the uncertainty in cumulative CO_2 leakage in the GCS site. The optimal monitoring design resulted in an uncertainty reduction in the cumulative leakage of CO_2 of approximately 73%. The proposed approach is efficient in developing monitoring designs under geologic uncertainty and enables safe geologic carbon sequestration operations.

1. Introduction

Geologic CO_2 sequestration (GCS) has emerged as an important technology to reduce anthropogenic greenhouse gas emissions to the atmosphere [1–8]. This has become increasingly popular worldwide due to the need to meet international climate protection agreements [9, 10]. Different types of underground formations have been proposed to store CO_2 emissions including oil and gas reservoirs, coal beds and seams, and deep saline aquifers [11]. The main concern in GCS projects is potential leakage of the CO_2 through leakage pathways, such as improperly abandoned wells, faults, and fractures [1, 12–15]. Such risks can pose a major threat to overlying resources (e.g., groundwater resources, oil and gas reservoirs, etc.) and human health [16, 17] Monitoring and verifying CO_2 behavior within the subsurface reservoir are crucial for detecting potential leakage, assessing storage capacity, and evaluating environmental impacts [18–20].

To ensure safe and efficient operations in a large-scale GCS site, risk management techniques are used to minimize and mitigate potential risks during CO_2 injection and post-injection periods [21–25]. Monitoring is thus an important aspect of GCS risk management, and one of the main goals of the Department of Energy (DOE) Office of Fossil Energy National Risk Assessment Partnership (NRAP) [26]. For this goal, several monitoring techniques have been developed, including near surface CO_2 flux and tracer measurements [27, 28], groundwater chemistry monitoring [29, 30], seismic surveying [28, 31–33], and pressure monitoring [34–38].

Optimal sensor placement and monitoring design play a critical role in achieving accurate and efficient monitoring in GCS projects. Depending on the reservoir properties and heterogeneity, the placement of monitoring wells can provide a more accurate measurement of the injected CO_2 plume and help mitigate potential leakage risks [39–42]. In common GCS operations, each injection well is paired with one monitoring well, though large-scale projects often incorporate a larger number of monitoring wells [43–45]. Moreover, the selection of monitoring measurement plays an important role in reducing uncertainties and quantifying risks in GCS operations [30, 46–49]. Therefore, it is crucial to define an optimal monitoring strategy in terms of both well placement and monitoring measurement type.

Recent advancement in monitoring systems such as smart or intelligent wells are capable of providing large amounts of data in terms of volume, velocity, variety, value, and veracity [50–52]. Classical techniques in data processing and forecasting are sometimes hindered by big data, therefore machine learning provides a promising approach to enhance data-driven subsurface energy resource systems [53–57]. By analyzing extensive data sets, machine learning algorithms can uncover complex latent patterns and relationships that may not be discernible through traditional methods [58–65]. Machine learning approaches, when combined with reduced-order modeling (ROM) techniques, enable efficient and accurate prediction of key parameters

[66–72], including pressure distribution, CO_2 plume migration, and reservoir behavior [73–77]. These insights facilitate the optimization of sensor placement and monitoring strategies, enabling better decision making and forecasting in GCS projects.

Accurately quantifying uncertainties is vital for the reliability of predictions and optimizing monitoring design under uncertain conditions [15, 39, 78–84]. Uncertainty quantification is particularly important in GCS due to inherent complexities and variabilities associated with subsurface conditions, fluid flow, and measurement errors [46, 85–87]. Several approaches for history matching or data assimilation have been applied to subsurface flow and transport, including Markov Chain Monte Carlo (MCMC) [61, 81, 82, 88, 89], randomized maximum likelihood (RML) [90], filter-based or rejection sampling (RS) [91–94], ensemble Kalman filtering (EnKF) [95–99] and ensemble smoother with multiple data assimilation (ES-MDA) [46, 100–105]. Filter-based approaches provide a robust framework for characterizing uncertainties associated with reservoir properties, operating conditions, and measurement errors, and with reduced complexity and cost compared to previously-mentioned techniques. Leveraging data assimilation techniques allows for informed risk assessment, ensuring the safety and efficiency of GCS projects.

Numerous research endeavors have been dedicated to addressing monitoring design, sensor placement, and uncertainty quantification in GCS. Previous studies have explored various modeling techniques, simulation frameworks, and optimization algorithms to enhance monitoring strategies and improve forecasting.

Efforts have been made to select the optimal monitoring measurements for GCS projects. Yonkofski et al. [49] use a simulated annealing (SA) global optimization approach to obtain the optimal monitoring measurement design in a GCS project. Their objective is to minimize the estimated time to first detection (ETFD) by iteratively mutating potential monitoring designs. Oladyshkin et al. [106] propose a polynomial chaos expansion (PCE) and bootstrap filtering approach for assimilating pressure data into reservoir models and quantifying the uncertainty reduction in CO_2 leakage rate at a GCS site. Liu and Grana [107] propose a deep convolutional autoencoder as a ROM strategy to assimilate seismic monitoring data in GCS. Their method requires HFS to obtain CO_2 saturation plume predictions from an ensemble of prior models, which is then used to calculate the seismic response. The autoencoder is used to project the observed monitoring measurements into latent space, where ES-MDA is used to update the model parameters and quantify the uncertainty in predictions.

Similar efforts have been made in the area of optimal monitoring well placement. Sun et al. [47] propose an approach to optimize monitoring well location based on pressure measurements for GCS under geologic uncertainty. Using binary integer programming problem (BIPP) formulation, they effectively select optimal monitoring locations for homogeneous and fluvial heterogeneous reservoirs. However, their method requires a large number of forward simulations, which can be computationally costly and time consuming. Sun and

Durlofsky [39] use a data-space inversion (DSI) approach to optimize the monitoring well locations in a GCS project with a genetic algorithm (GA) global optimization. Using principal component analysis (PCA) as a model reduction strategy, they reduce the uncertainty in CO_2 saturation plume using a RML approach. In this approach, posterior geological models are not generated in the DSI method, which is different from traditional ensemble-based data assimilation approaches.

Besides optimal well placement and monitoring measurement selection, several research studies have been conducted to quantify the uncertainty in GCS projects. Jia et al. [85] propose a Bayesian model average and Monte Carlo simulation to quantify parameter uncertainty based on a PCE ROM. However, Monte Carlo strategies require a very large number of realizations and can be extremely computationally inefficient. Chen et al. [46] propose a risk assessment approach using ES-MDA with geometric inflation factors (ES-MDA-GEO) to quantify the uncertainty monitoring data and calibrate the prior uncertain geologic models. Their work leverages continuous data assimilation as new monitoring data becomes available in GCS projects to improve the underlying model and reduce uncertainties. Mehana et al. [108] provide a ROM-based approach to quantify wellbore leakage from depleted reservoirs in CO_2-EOR operations. They compare the performance of different machine learning-based ROMs for prediction of cumulative leakage and quantify the uncertainty using Monte Carlo simulations. Pawar et al. [109] provide a robust framework for quantitative risk assessment of leakage in GCS. Utilizing the NRAP-open-IAM (Integrated Assessment Model) tool, they are able to quantify the leakage risk through legacy or abandoned wells in large-scale GCS projects. This framework can then be used to support permit applications for GCS projects.

In this paper, we build upon the work of Chen et al. [110] to systematically design an optimal monitoring placement and measurement strategy for large-scale GCS beyond naive monitoring well placement and monitoring design. Chen et al. [110] developed a robust framework for uncertainty reduction in cumulative CO_2 using Multivariate Adaptive Regression Splines (MARS) [111]. Using a filter-based data assimilation process, they quantify the uncertainty reduction in cumulative CO_2 leakage. However, their work assumes a predetermined, uninformed placement of the monitoring well and monitoring measurement type, relying solely on engineering judgement and fixed monitoring configurations.

We propose a method for optimal GCS monitoring design based on well placement optimization and monitoring measurement selection. We develop an artificial neural network ROM to predict cumulative CO_2 leakage from a prior ensemble of uncertain model parameters, and implement a filter-based data assimilation approach to select the most informative monitoring well location and measurement type in order to reduce uncertainties and CO_2 leakage risks. The structure of this paper is as follows: Section 2 present our methodology, Section 3 presents the results of our approach for two synthetic cases, and Section 4 summarizes our findings, discusses their implications, and outlines potential avenues for future research in the field of GCS.

2. Methodology

In this section we will discuss the approaches for uncertainty quantification, ROM development, ROM training and performance, and optimal monitoring workflow design.

2.1 Uncertainty Quantification

The goal of this study is to evaluate the value of data in GCS monitoring design. The value of data is quantified by the amount of uncertainty that is reduced in the cumulative CO_2 leakage, M_c, over the duration of a GCS project. The prior probability density function (PDF) of the cumulative CO_2 leakage is denoted as $P(M_c)$. In this study, prior refers to the probability distribution before a monitoring program is implemented. The distribution of potential monitoring data that could be measured at the monitoring wells is denoted as $D = [d_1, d_2, \ldots, d_{n_d}]$, where $\{d_i\}_{i=1}^{n_d}$ are the individual monitoring data points obtained if a monitoring design were implemented in a particular leakage scenario and n_d is the total number of monitoring data points in D. In this study, monitoring data is sampled monthly, and can represent pressure, CO_2 saturation, or temperature values at the monitoring well. Thus, we denote D^j as the j^{th} realization of D. For each D^j, we obtain a posterior PDF denoted by $P(M_c|D^j)$, which can be calculated using a data assimilation procedure as the cumulative CO_2 leakage, M_c, for a given monitoring design data D^j. The objective is to quantify the value of information (VOI) estimated from a distribution of potential monitoring design, allowing us to choose an optimal monitoring well placement and monitoring measurement type to minimize the uncertainty in potential leakage scenarios. Following Chen et al. [81, 110] and Le and Reynolds [112], the VOI is quantified by the uncertainty reduction in the objective function. We denote the amount of uncertainty in cumulative CO_2 leakage distribution $P(M_c)$ as $U[P(M_c)]$, defined as:

$$U[P(M_c)] = P_{90}[P(M_c)] - P_{10}[P(M_c)] \tag{1}$$

where $P_{10}[\bullet]$ is the 10^{th} percentile of a distribution and $P_{90}[\bullet]$ is the 90^{th}. The distribution of cumulative CO_2 leakage can be attributed to the uncertainty in model parameters, in this case the number of and the vertical transmissibility of potential leaky pathways, k_v^ℓ, and the reservoir permeability multiplier, k_R. Therefore, selecting a monitoring design that reduces the uncertainty in M_c ensures that the monitoring design will function effectively under multiple possible potential leakage scenarios.

The expected posterior uncertainty distribution in M_c given D is given by:

$$E_d[U[P(M_c|D]] = \frac{1}{\ell_d}\sum_{j=1}^{\ell_d} U[P(M_c|D^j)] \tag{2}$$

where E_d is the expectation with respect to all realizations of D and l_d is the number of data realizations. The expected uncertainty reduction, U_R, as a result of data acquisition from a potential monitoring design is given by the difference between the prior uncertainty and the expected posterior uncertainty in cumulative CO_2 leakage, as defined by:

$$U_R = U[P(M_c)] - E_d[U[P(M_c|D)]] \tag{3}$$

By selecting the optimal monitoring well placement and monitoring measurement type, the uncertainty reduction, U_R, quantifies the effectiveness of the particular GCS monitoring design, where the higher the uncertainty reduction the higher the VOI in the monitoring data obtained in the monitoring design.

2.2 Reduced Order Model Development

Given the computational cost of traditional filter-based data assimilation, a reduced-order model is developed in this study. The workflow for the ROM development is illustrated in Fig.1 This section provides a summary of the main steps in the ROM development workflow:

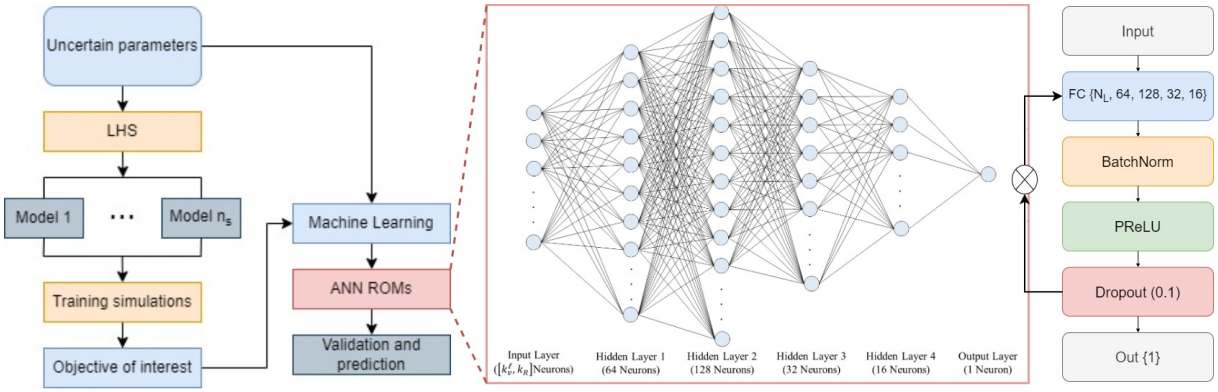

Figure 1: Workflow diagram for machine learning-based ROM development.

Step 1: *Experimental design*: Given a set of uncertain parameters $k_v^{\ell_d}$ and k_R, we generate n_s training samples using Latin Hypercube Sampling (LHS) [113, 114].

Step 2: *Forward simulations*: Physics-based HFS of CO_2 injection and post-injection migration is performed with each of the n_s training samples using the Finite Element Heat and Mass Transfer (FEHM) simulator [115].

Step 3: *Collect training data*: For each training realization, the set of uncertain parameters, monitoring data, and cumulative CO_2 leakage are collected. In Fig.1, we see that the uncertain parameters are inputs for the ROM training and the objectives of interest (cumulative CO_2 leakage and monitoring data) are the

corresponding outputs.

Step 4: *Train ROMs for the objectives of interest*: A reduced-order model is used to map the relationship between the training parameters inputs and outputs. We build an ensemble of ROMs, one for each objective of interest, namely the cumulative CO_2 leakage (M_c) and the simulated monitoring data (D) at each specified timestep. A fully-connected artificial neural network (ANN) is implemented to build the ROMs. Fig.1 shows the architecture of the ANN.

Step 5: *Validate the ROMs against the HFS*: Using 10-fold cross-validation [116], we test the predictions from the ROMs against the HFS results in order to perform hyper-parameter tuning and obtain robust ROMs that can be used for further predictions.

Using the Python TensorFlow/Keras package [117, 118], we develop a fully-connected ANN architecture to build the ROMs. Each ANN consists of four hidden layers with sizes 64, 128, 32, and 16, respectively, with a total number of parameters equal to $14,705$. A kernel regularizer is applied with the ℓ_1-norm, and dropout of 10% is used on each hidden layer. The activation function is the parametric rectified linear unit (PReLU), which learns the negative slope for each batch in each epoch. The Adam optimizer [119] is used with a mean squared error (MSE) loss function. Training is performed on an NVIDIA RTX A6000 GPU in about 2 minutes for each ROM using 10-fold cross-validation. The average validation MSE is approximately 8.5×10^{-4} and the correlation coefficient (R^2) is approximately 0.98. The truth vs. prediction performance for a set of 500 realizations of uncertain parameters is shown in Fig.2.

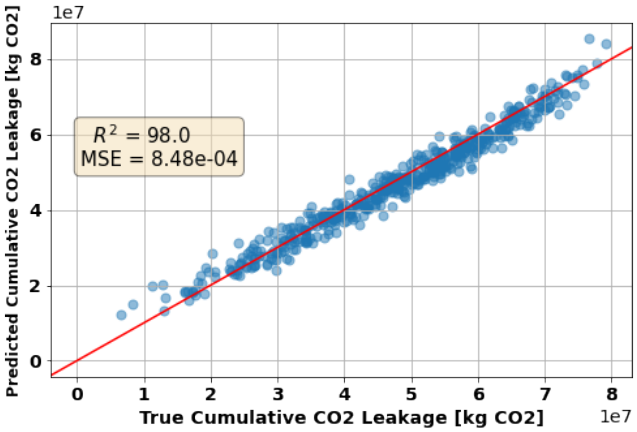

Figure 2: Cumulative CO_2 leakage prediction from ANN ROM vs true cumulative CO_2 leakage.

2.3 Workflow for optimal monitoring design

In this section we present a filtering and ROM based workflow for optimal monitoring design of GCS. The workflow diagram is shown in Fig. 3. The main steps for the optimal monitoring design workflow are

summarized below.

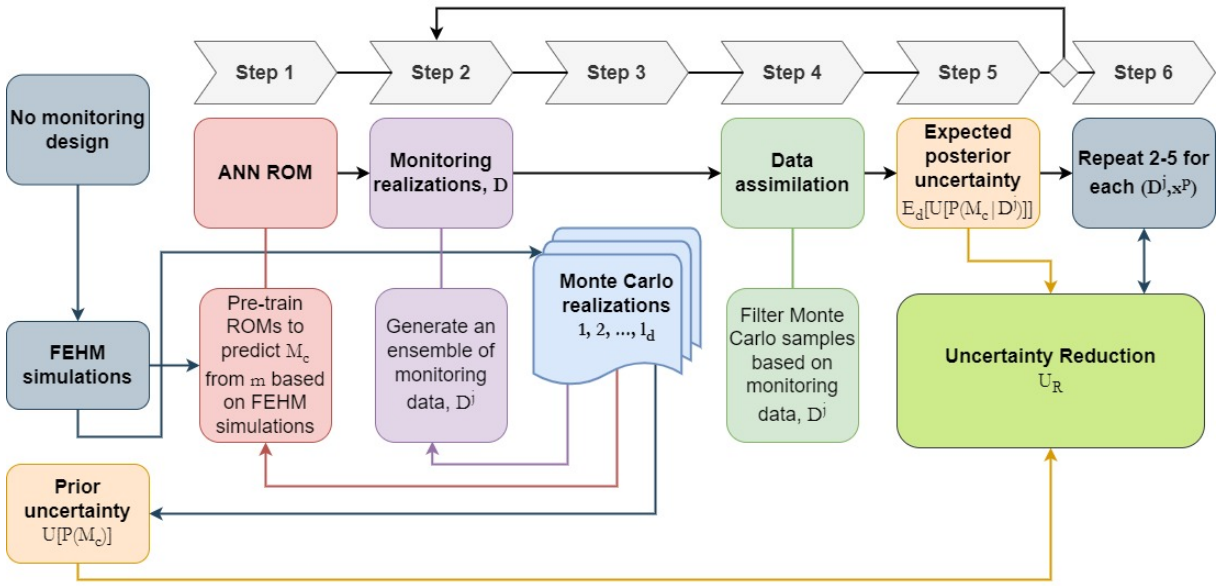

Figure 3: Workflow diagram for optimal monitoring design. First, calculate the prior uncertainty with no monitoring design based on Monte Carlo samples of the FEHM simulations. Then use the pre-trained ROMs to predict CO_2 cumulative leakage using Monte Carlo samples and perform data assimilation of monitoring measurement D^j for monitoring well placement x^p to compute expected posterior uncertainty. The uncertainty reduction for case (D^j, x^p) is given by $U^{x_p}[P(M_c)] - E_d[U^{x_p}[P(M_c|D^j]]$, and we repeat for each possible D^j and x^p.

Step 1: *Develop ROMs for the objective function, M_c, and predict monitoring data, D*: A detailed description of the ROM development workflow were presented in the previous section. We build one ROM for each monitoring data point, d_i, in each data vector D^j. The vector of predicted monitoring data is denoted as $O(m) = [O_1(m), O_2(m), \ldots, O_{n_d}(m)]^T$, where m is the vector of uncertain model input parameters, namely k_v^ℓ and k_R. The ROMs are used to replace FEHM physics-based simulations and to predict the objectives of interest for a set of new input parameters not in the training data.

Step 2: *Generate an ensemble of realizations of monitoring data, D*: Initially, l_d realizations are sampled from the prior PDF of m, and are denoted as $\{\widetilde{m}^j\}_{j=1}^{\ell_d}$. The corresponding monitoring data, $\widetilde{d}_{obs}^j$, for each $\widetilde{m}^j$ are given by:

$$\widetilde{d}_{obs}^j = O(\widetilde{m}^j) + e^j \tag{4}$$

where $O(\widetilde{m}^j$ is the ROM prediction for n_d monitoring data points and e^j denotes the j^{th} realization of measurement errors which follow a Gaussian distribution.

Step 3: *Generate Monte Carlo samples, and calculate prior uncertainty*: A large number $(50,000)$ Monte Carlo samples are generated from the prior distribution of m, and denotes as $\{\hat{m}^k\}_{k=1}^{\ell_{MC}}$. The Monte Carlo samples are used to calculate the prior PDF and the amount of uncertainty in the prior can be computed

using Eq. (1).

Step 4: *Filter the Monte Carlo samples, and compute expected posterior uncertainty*: Using a filtering-based method [94], also known as rejection sampling, we construct a posterior distribution of m conditional to each $\widetilde{d}^j_{obs}$. First, using the Monte Carlo samples, $\hat{m}^k$, generated in Step 3, we simulate the corresponding monitoring data $\hat{d}^k$ with the ROMs generated in Step 1, such that $\hat{d}^k = O(\hat{m}^k)$. Here, $\hat{d}^k$ represents a realization from the distribution of potential monitoring data sets that capture potential CO_2 leakage scenarios given the uncertain input parameters k_v^ℓ and k_R. The data assimilation error is defined as the maximum absolute error (MAE) as follows:

$$MAE(d^j_{obs}) = \max_{1 \leq i \leq n_d} |\widetilde{d}^j_{obs,i} - \hat{d}^k_i| \tag{5}$$

Given a threshold value τ, the $\hat{m}^k$ sample is accepted as a legitimate realization of the posterior distribution according to the following acceptance probability:

$$P_{acc}(\hat{m}^k) = \begin{cases} 1, & \text{if } MAE < \tau \\ 0, & \text{otherwise} \end{cases} \tag{6}$$

The threshold value, τ, is chosen based on engineering judgement and takes into consideration the measurement and modeling errors. Therefore, $\hat{m}^k$ is accepted if it is deemed sufficiently consistent with the true monitoring data realization. Every Monte Carlo sample is evaluated using Eq. (6) and the accepted samples constitute the posterior distribution of m conditional to the monitoring data realization $\widetilde{d}^j_{obs}$ such that ℓ_d posterior samples of m are obtained. The expected posterior uncertainty is calculated using Eq. (2).

Step 5: *Calculate the expected amount of uncertainty reduction U_R*: The expected amount of uncertainty reduction, U_R, is calculated by comparing the uncertainty in the prior distribution and the expected value of the uncertainty in the posterior distribution using Eq. (3).

Step 6: *Monitoring well placement optimization*: We repeat Steps 2-5 for every possible monitoring well location in the GCS area of review (AOR), conditional to the data for each possible measurement type, D^j. In order to accelerate the optimization procedure, we coarsen the simulation grid into a 4×4 subgrid, meaning there are 16 possible monitoring well locations. We calculate the expected amount of uncertainty reduction for each monitoring data type, D^j, for each possible monitoring well location $\{x^p\}_{p=1}^{16}$, and obtain the monitoring design that maximally reduces the uncertainty in cumulative CO_2 leakage (maximally reducing the uncertainty is equivalent to minimizing the negative expected uncertainty reduction), as shown in Eq.

(7)

$$x_p^* = \min_{1 \leq p \leq 16} -U_R^{x_p} \tag{7}$$

This results in an exhaustive search in the subgrid to obtain the optimal well location, x_p^*, that yields the highest uncertainty reduction, defined by $U_R^{x_p}$ as follows:

$$U_R^{x_p} = U^{x_p}[P(M_c)] - E_d[U^{x_p}[P(M_c|D^j]] \tag{8}$$

With this optimal monitoring design workflow, the expected uncertainty reduction in cumulative CO_2 leakage for each potential monitoring measurement and each potential monitoring well location can be computed, and the optimal monitoring design that reduces the uncertainty in the simulated amount of CO_2 leakage is obtained.

2.4. Model Description

We implement the optimal monitoring design workflow on a synthetic GCS model consisting of a heterogeneous storage reservoir, a homogeneous caprock layer and a homogeneous aquifer, as shown in the schematic of the base model in Fig. 4. The thickness of each of the three layers is 30 m, and the model is 1 km wide in the horizontal dimensions. The depth from ground surface to the top of the model is 1000 m. A CO_2 injection well is placed at the center of the reservoir and multiple potential leakage pathways traverse the caprock, where CO_2 could potentially leak into the aquifer. Note that only one possible leakage pathway is shown in Fig. 4, while we have considered several scenarios with multiple potential leakage pathways. The caprock and aquifer layers have a homogeneous permeability distribution equal to 1×10^{-1} m^2 and 1×10^{-13} m^2, respectively. The storage reservoir has a heterogeneous permeability distribution, as shown in Fig. 5. The base model is generated using a spherical variogram model [120, 121] with major and minor correlation lengths of 680 m and 280 m, respectively, with a major direction of 45° from the positive x-axis.

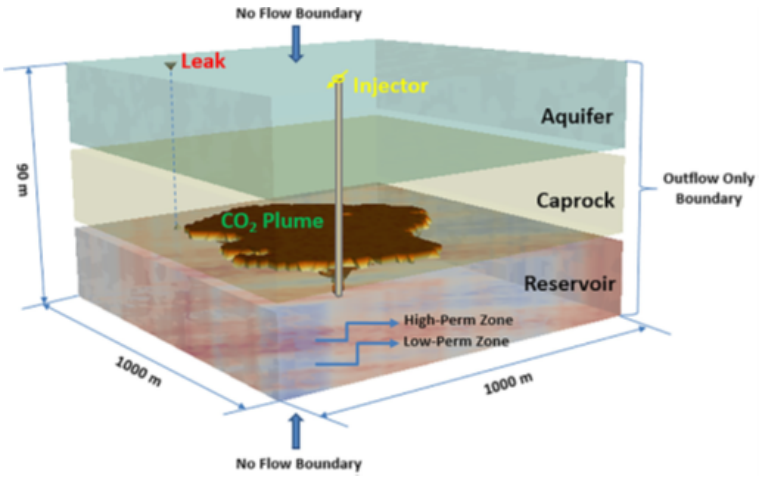

Figure 4: Schematic of the base model, in which a storage reservoir and aquifer are separated by a caprock. At the center is a CO_2 injection well. The vertical axis is exaggerated 7 times.

The mean of the permeability field is 1×10^{-13} m^2. For each realization, we assume that the reservoir permeability is uncertain, and to honor this uncertainty we use a permeability multiplier, k_R, to multiply the aforementioned base permeability distribution. The lower and upper bounds for the multiplier k_R and the potential leaky pathways k_v^ℓ are shown in Table 1.

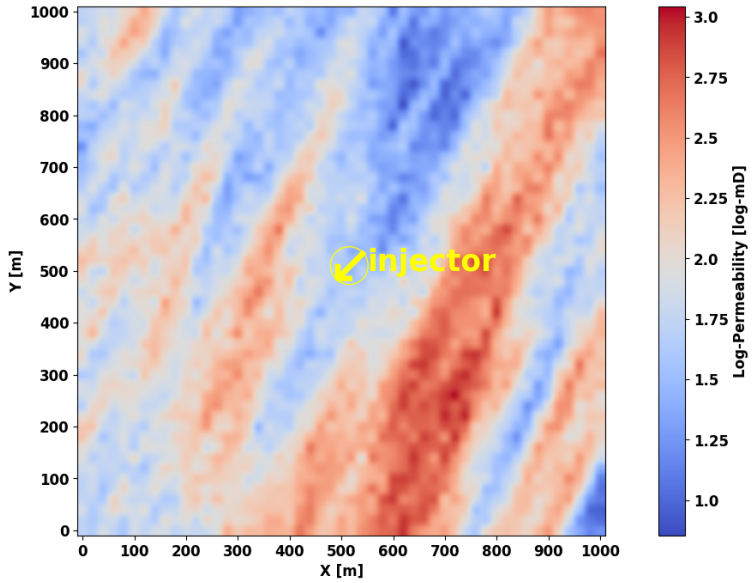

Figure 5: Log-permeability distribution of the base model. The darkest blue color corresponds to the lowest permeability, while the darkest red color corresponds to the highest. The yellow circle with an arrow indicates the CO_2 injection well.

A numerical mesh for the reservoir simulation is made using the grid generation toolkit *LaGriT* [122]. The numerical mesh has 51 grid nodes in both the x- and y-directions, and 31 grid nodes in the z-direction.

Table 1: Uncertain parameters and their lower and upper bounds

Uncertain parameters	Symbol	Lower bound	Upper bound	Unit
Reservoir permeability multiplier	k_R	0.5	2	–
Permeability of leaky pathway(s)	k_v^ℓ	-19 0.001	-14 10	$log_{10}\ [m^2]$ mD

The distance between each grid node in the x- and y-directions is 20 m, and in the z-direction it is 3 m. The total number of grid nodes used in the simulation is 80,631, with 26,010 grid nodes in the reservoir and caprock, respectively, and 28,611 grid nodes in the aquifer. FEHM is used for 3D multi-phase flow simulations [115]. The boundary conditions of the reservoir are defined as Dirichlet boundaries, allowing CO_2 to flow out but not in, and water pressure above hydrostatic. The top and bottom boundary conditions of the simulation model are no-flow boundaries. The thermal conditions of the model are initialized using a geothermal gradient of 0.03°C/m with a temperature of 20°C at the top. Pressure gradients are initialized at 9.81×10^{-3} MPa/m with a pressure of 0.2 MPa along the top. In this study, CO_2 is constantly injected in a five-year period, monitored monthly, with a constant injection rate of 0.1 million metric tons/year.

3. Results

In this section we apply our optimal monitoring design workflow using the ANN ROMs and filter-based uncertainty quantification approach to obtain the optimal monitoring well placement and monitoring measurement data type for two synthetic GCS examples.

3.1 Workflow validation

We validate the workflow for optimal GCS monitoring design using a simple example. Fig. 5 shows the log-permeability distribution for the base model with a CO_2 injection well at the center, noted with a yellow circle and arrow. All the monitoring data in this study are collected in the aquifer zone, similar to monitoring at the above zone monitoring interval (AZMI) in the work of Sun et al. [47]. The monitoring frequency is once per month for the duration of 5 years injection, resulting in 60 monitoring data points. The objective function, M_c, is the cumulative CO_2 leakage at the end of 5 years. In the model, we set up three material zones corresponding to the three adjacent formations, namely the storage reservoir, caprock, and aquifer. The cumulative CO_2 saturation in each zone can be output from the FEHM simulation results, and the cumulative leakage is computed by summing the CO_2 mass in the aquifer and caprock layers. Our approach for monitoring design involves quantifying the uncertainty reduction by monitoring pressure, CO_2 saturation,

or temperature at each potential monitoring well location.

The data assimilation error tolerance, τ from Eq. (6), for pressure is set equal to 0.002 MPa, while for CO_2 saturation it is 0.05, and for temperature it is 0.002°C. Note that the choice of τ is site and case specific and is based on engineering judgement that takes into consideration the measurement and modeling error.

Two case studies are considered in this study: (1) GCS project with 3 potential leakage pathways, and (2) GCS project with 6 potential leakage pathways. The uncertain parameters are the permeability multiplier, k_R for the storage reservoir, and the ℓ permeability values for the ℓ potential leakage pathways, where $\ell = 3$ and $\ell = 6$, respectively. The total number of uncertain parameters, u^ℓ are 4 and 7, respectively. The lower and upper bounds for the uncertain parameters are shown in Table 1. For each case study, we run 500 training simulations generated by LHS with u^ℓ uncertain parameters. Each HFS requires approximately 22 minutes. We perform parallelization on an 8-node cluster, and the total simulation time is approximately 23 hours to finish all 500 training realizations. Fig. 6 shows the base model for Case 1 and Case 2 respectively.

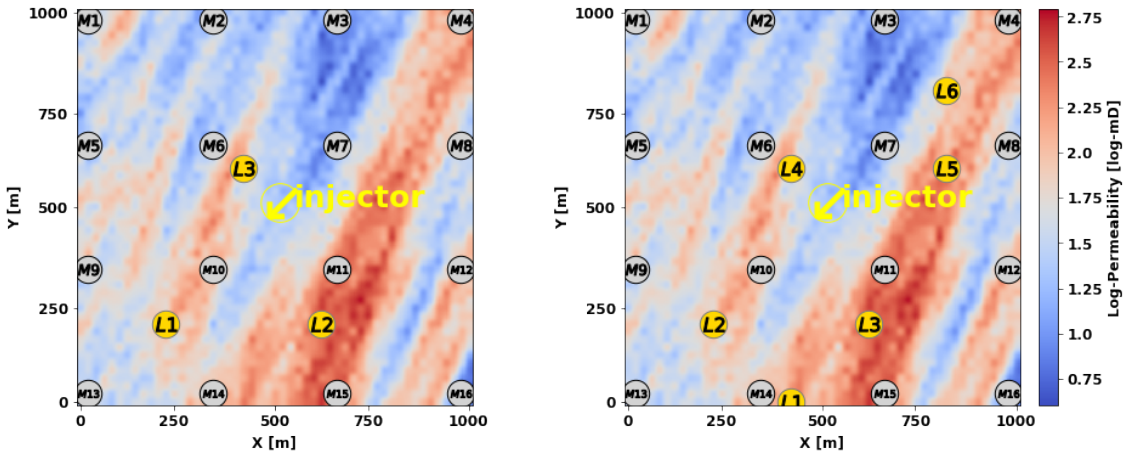

Figure 6: Log-permeability distribution of the base model for Case 1 (left) with 3 potential leaky pathways, and Case 2 (right) with 6 potential leaky pathways. The dark yellow circles labeled L_i represent the leakage pathways, light gray circles labels M_i are the possible monitoring well locations, and the yellow circle with an arrow is the CO_2 injection well.

We choose one simulation from the 500 training realizations in Case 1 to show when CO_2 leakage occurs. The values of the different parameters for the chosen model are shown in Table 2. The cumulative CO_2 leakage over the GCS project time is shown in Fig. 7. Figure 8 shows the leaked CO_2 saturation distribution at the top of the aquifer. It can be seen that CO_2 leakage occurs after about 210 days of injection. We observe that CO_2 is leaking through the potential pathway L_3, which is 141.4 m away from the injector, while no leakage occurs at potential pathways L_1 and L_2 after 5 years of injection. For this specific example, it is important to note that the permeability of L_3, k_v^3 is higher than that of L_1 and L_2.

Table 2: The parameters for one chosen model from the 500 training realizations in Case 1

Parameters	Value	Unit
CO_2 injection rate	3.17	kg/s
Thickness of caprock layer	30	m
Permeability of 1^st potential leakage pathway	2.19×10^-17	m^2
Permeability of 2^nd potential leakage pathway	3.37×10^-17	m^2
Permeability of 3^rd potential leakage pathway	2.97×10^-16	m^2
Distance between injector and 1^st potential leakage pathway	424.3	m
Distance between injector and 2^nd potential leakage pathway	360.6	m
Distance between injector and 3^rd potential leakage pathway	141.4	m
Permeability for aquifer layer	1×10^{-13}	m^2
Permeability for caprock layer	1×10^{-19}	m^2
Reservoir permeability multiplier	1.88	–

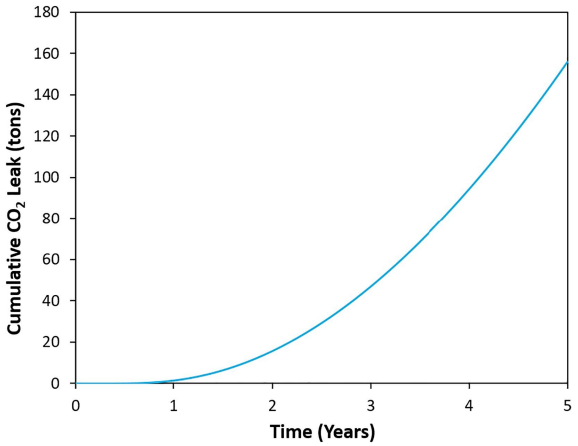

Figure 7: Cumulative CO_2 leakage over time computed for one chosen training realization in Case 1.

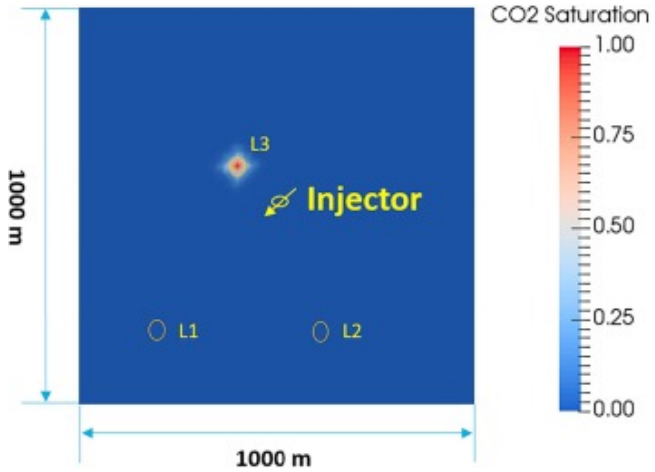

Figure 8: Plan view (top of the aquifer) of CO_2 leakage at the end of 5 years of injection based on one chosen training realization in Case 1. Yellow circles indicate the potential leakage pathways. Units for CO_2 saturation is fraction.

For each case, the 500 training realizations are used to train ROMs for the monitoring data and cumulative CO_2 leakage using the ANN architecture in Fig 1. Fig. 2 shows the quality of the ROMs tested by 10-fold cross-validation [116, 123]. The MSE and R^2 are 8.5×10^{-4} and 0.98, respectively. This proves that the fidelity of ROMs to the numerical simulations is high at the advantage of a much lower computational cost.

With the proposed workflow, the expected uncertainty reduction of the cumulative CO_2 leakage can be computed for each of the 16 possible monitoring well locations, for each monitoring measurement type. For each data set, 200 possible realizations of monitoring data are generated following Step 2 in Section 2.4. To obtain the expected uncertainty reduction using Eq. (3), the prior uncertainty $U[P(M_c)]$ and posterior uncertainty $U[P(M_c|D^j)]$ corresponding to each possible monitoring data realization D^j for each possible well location x^p should be computed. Higher uncertainty reduction of the objective function indicates greater VOI in the monitoring data obtained from the optimal well location and monitoring measurement type. Through these examples, we can see that our proposed workflow can be effectively used to determine optimal CO_2 monitoring design from a set of alternative monitoring designs.

We observe that monitoring for pressure provides the highest uncertainty reduction in general, followed by CO_2 saturation and lastly pressure. The spatial distribution of uncertainty reduction in CO_2 leakage is shown in Fig. 9 for every possible well location x^p in the 4×4 subgrid, and point-wise comparison of the uncertainty reduction at each monitoring well location for each measurement type is shown in Fig. 10. One can observe that placing a monitoring well at location 6 and assimilation the pressure measurements provides the highest uncertainty reduction possible in the monitoring design for both Case 1 and Case 2. For Case 1, the optimal monitoring design given by $(pressure, x^6)$ yields an uncertainty reduction in the cumulative leakage of CO_2 of approximately 29.42×10^3 metric tons (29.24 kt), while the optimal design for CO_2 saturation and temperature monitoring yield an uncertainty reduction of approximately 19.34 kt and 17.71 kt, respectively. Similarly, for Case 1, the optimal monitoring design given by $(pressure, x^6)$ yields an uncertainty reduction of 26.29 kt of cumulative CO_2 leakage, while the optimal design for CO_2 saturation and temperature monitoring yield an uncertainty reduction of approximately 16.94 kt and 16.29 kt, respectively.

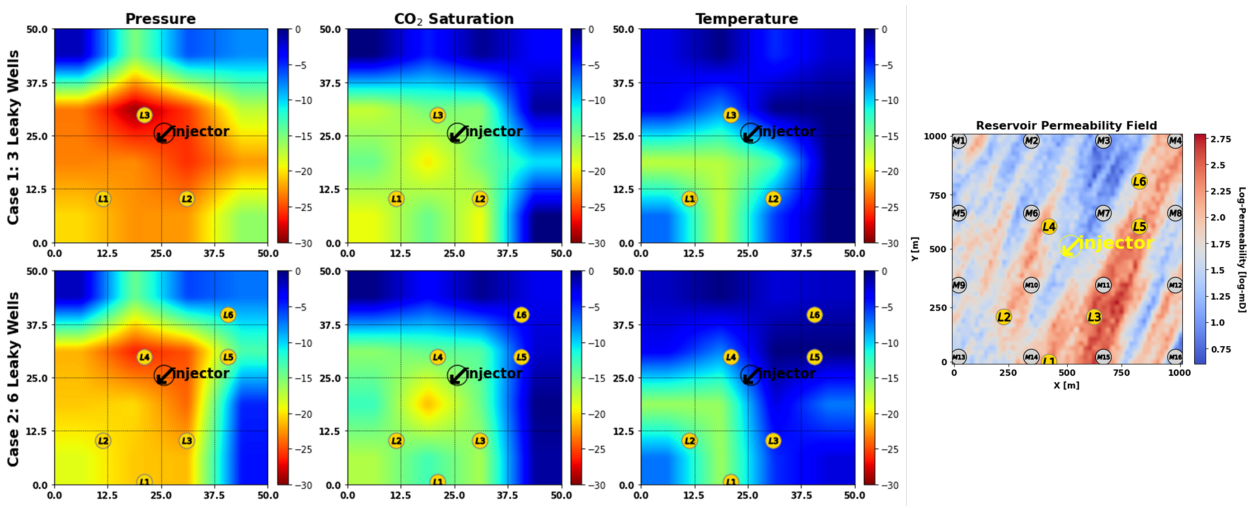

Figure 9: Left: Plan view (top of the aquifer) of the uncertainty reduction obtained by all possible monitoring well locations. Top row represents Case 1 with 3 leakage pathways, and the bottom row represents Case 2 with 6 leakage pathways. Each column represents monitoring data for pressure, CO_2 saturation, and temperature, respectively. Right: Plan view of the reservoir permeability field with possible leakage pathways (yellow) and all possible monitoring well locations (gray).

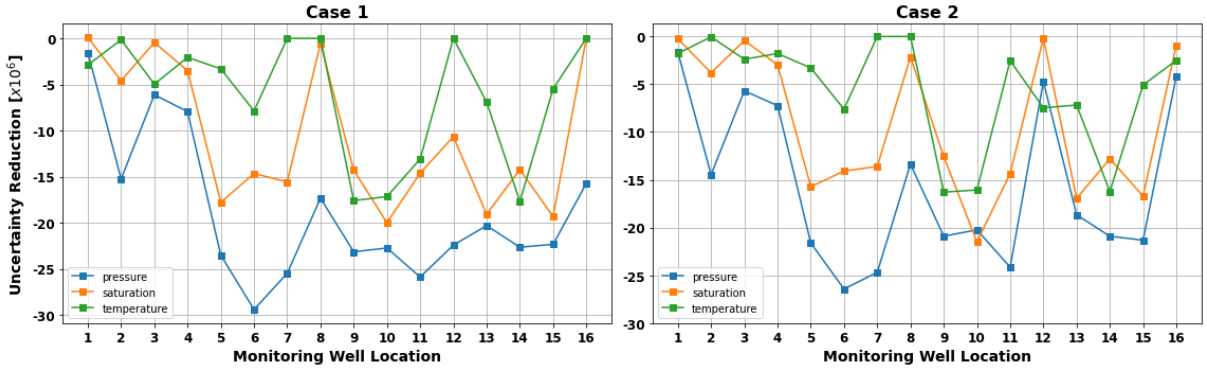

Figure 10: The point-wise calculated uncertainty reduction at each possible monitoring well location for each measurement type. Case 1 is shown on the left, and Case 2 on the right.

The histograms for the prior and posterior distributions of the objective function obtained from the data realizations 1 and 100 for Case 1 and 2, respectively, are show in Fig. 11. The prior distribution is generated using LHS from the set of uncertain input parameters, k_V^ℓ and k_R, with a uniform distribution and calculating the cumulative CO_2 leakage using the ROMs. The posterior distribution for two random realizations, namely realization 1 and 100, are shown. These two are selected given that they had a relatively high amount of cumulative CO_2 leakage. Recall that the total uncertainty reduction, U_R is given by the difference between the expected posterior uncertainty (the expected value of the ensemble of realizations) and the prior uncertainty distribution. The variances of the posterior distributions calculated show significant reduction in uncertainty of cumulative CO_2 leakage compared to the priors. The optimal monitoring design

$(pressure, x^6)$ yields a reduction in cumulative CO_2 leakage uncertainty of approximately 29.24 kt.

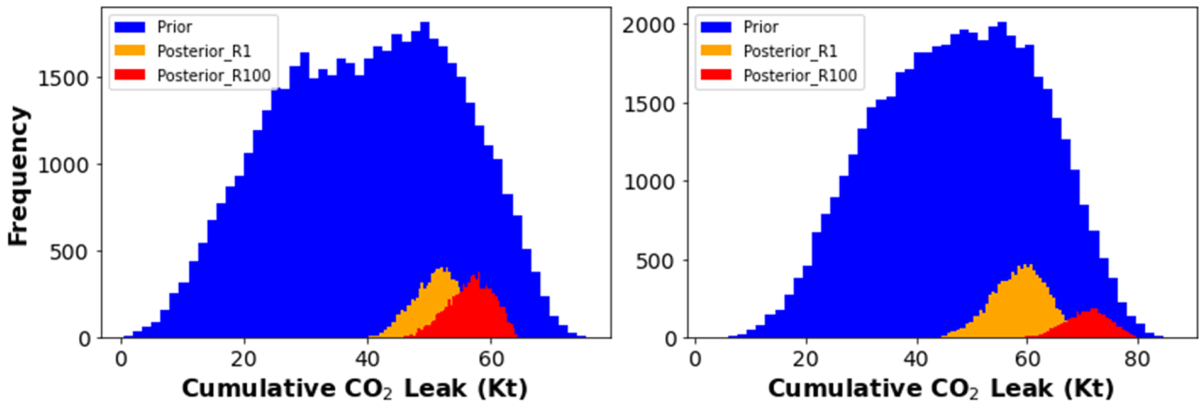

Figure 11: The histograms for the prior (blue) and posterior distributions obtained at the optimal monitoring design from the data realizations 1 (orange) and 100 (red) for Case 1 (left) and Case 2 (right), respectively.

3.2 Discussion

GCS monitoring operations require detailed data processing and interpretation in order to accurately quantify and potentially minimize leakage risks. Associated costs of performing monitoring operations requires evaluating the potential value of monitoring measurement type, and optimal monitoring well location, before the actual monitoring strategy takes place in the field. The workflow proposed can be used to select an optimal monitoring design that is robust under multiple potential leakage scenarios. Previous efforts in characterizing the geologic uncertainty in GCS projects show the importance and effect of these parameters [46, 85, 109], selecting the optimal measurement type [49, 106], or selecting the optimal monitoring well location [39, 47]. Our work provides a framework to unify these three concepts under a single optimal monitoring design framework.

The slight difference in uncertainty reduction between Case 1 and Case 2, despite the fact that we have more leakage pathways, can be attributed to the fact that the main source of uncertainty is the geologic parameters, namely k_v^ℓ and k_R, rather than the number of leakage pathways. These parameters ultimately control the leaking of CO_2, and can range between very small ($\sim 0.001mD$) to medium ($\sim 10mD$). Thus, the cumulative CO_2 leakage does not directly correlate with having more or less leakage pathways, but with the permeability of the leakage pathways, k_V^ℓ, and the reservoir permeability multiplier, k_R. For instance, wells 6-7 and 10-11 lie closest to the injection well at approximately 176.8 m, yet well 6 yields the highest uncertainty reduction since it is closest to a high permeability streak, similar to well 11. On the other hand, wells 7 and 10 lie on low permeability streaks, making the plumes travel relatively slower. Therefore, distance from injector and leakage pathways is important, but mostly controlled by the permeability heterogeneity in

the reservoir.

Furthermore, it is evident that monitoring for pressure data yields the highest uncertainty reduction out of the three possible measurement types. This is due to the fact that the pressure plumes travel the fastest along a given subsurface formation, followed by saturation plumes and temperature plumes, in that order [32]. Temperature plumes tend to travel the least, given the thermal equilibrium of deep underground formations and the gradual enthalpy change in the reaction of CO_2 in saline aquifers [124]. In some monitoring locations, such as wells 7 and 8, monitoring for temperature provides little to no uncertainty reduction whatsoever, while pressure monitoring yields about 17-25 kt reduction. The total uncertainty reduction given by the sum of all three measurements correlated primarily with the pressure monitoring data, and assimilating multiple measurements types simultaneously does not necessarily add linearly, and tends to be dominated by a single measurement. Refer to Chen et al. [110] for more information on assimilating multiple measurement types simultaneously.

It is also important to note that the monitoring wells are only drilled through the aquifer, and not the caprock and reservoir, thus only collecting monitoring measurements at the aquifer zone. This is way, despite x^6 being further away from the injector than the closest leakage pathway (L_3 in Case 1 and L_4 in Case 2), it still provides the most information about CO_2 leakage into the aquifer zone. Also, recall the aquifer is geologically homogeneous, and the pressure, CO_2 saturation, and temperature response does not necessarily exactly correlate with the reservoir response.

Regarding the monitoring well location grid, location x^6 yields the highest uncertainty reduction when using pressure measurements for both Case 1 and Case 2. However, the 16 possible monitoring well locations exist on a coarse 4×4 subgrid. Monitoring location x^6 is closest to the injection well and a leakage pathway in both Case 1 and Case 2, and therefore provides the best uncertainty reduction. However, if a finer monitoring well location grid were used, say 16×16 or 32×32 (which is still coarser than the simulation grid at 51×51), a location between the injector well and L_3 in Case 1 and L_4 in Case 2 would most likely yield the best uncertainty reduction. This is due to the fact that a monitoring well in that location would be able to detect the CO_2 plume before it even reaches and leakage pathways, and would still be in the region of high permeability in the reservoir, thus yielding the best uncertainty reduction in cumulative CO_2 leakage.

Moreover, given that we are using a coarse monitoring well location grid, several locations such as $M_{1-4}, M_8, M_{12}, and M_{14-15}$ yield little to no uncertainty reduction. We stipulate that this occurs because the CO_2 plume reaches the leakage pathways before it reaches these monitoring wells, and therefore provide little information to the data assimilation to reduce the uncertainty in leakage. This also leads to the idea that most of the CO_2 leakage is occurring in the pathways closest to the injection well, and thus the closer monitoring locations provide a better uncertainty reduction than those in the boundaries or further away.

This relates to the fact that despite Case 2 having more leakage pathways, the uncertainty reduction in kt of CO_2 is not much different from that of Case 1.

Even though the examples used in our study to demonstrate how monitoring data from a shallow aquifer can be used, the proposed workflow can be extended and applied to monitoring data collected at any location and time within the GCS project. The potential value of such monitoring data can be evaluated by the presented workflow. Furthermore, placing several monitoring wells can provide a slight advantage compared to a single injector-monitor pair, but is impractical in field applications. Moreover, using several monitoring measurement types simultaneously provides little to no advantage compared to pressure monitoring. Refer to Chen et al. [110] for further details.

At a CO_2 storage field operation, an optimal monitoring schedule and location based on the VOI described in this work can be used to collect the best possible monitoring data. The monitoring data can be assimilated to calibrate the uncertain model parameters using traditional data assimilation methods such as EnKF [125] or ES-MDA [126]. The calibrated models can be used to improve the accuracy in prediction for future and long-term behavior of the injected CO_2.

4. Conclusions

In this study, a workflow based on a machine learning reduced-order modeling technique and uncertainty quantification method within an optimization loop is proposed for geologic CO_2 sequestration monitoring design. We use the uncertainty reduction in cumulative CO_2 leakage as the quantity of interest to measure the potential value of monitoring measurement data. The optimal monitoring design yields an uncertainty reduction of approximately 29.94 kt in CO_2 leakage. The following conclusions have been drawn from this research:

1. The proposed workflow can generate reasonable values of uncertainty reduction in different risk metrics at CO_2 storage site, including cumulative CO_2 leakage by utilizing different monitoring designs and has been demonstrated using a synthetic GCS project. The optimal monitoring design is obtained my assimilating pressure data at monitoring well location 6.

2. The effect of different types of measurements (pressure, CO_2 saturation, and temperature) and the effect of monitoring well location on the choice of monitoring design is investigated. It is observed that pressure data has more value of information compared to CO_2 saturation, while temperature has the least value of information, though still valuable in terms of uncertainty reduction compared to no monitoring strategy.

3. Well placement optimization is important to maximize the value of information for the monitoring design. Typical operations include pairs of one monitoring well for each injection well, partly due to the cost of drilling and data acquisition. Determination of the best location provides significant benefits in reducing the uncertainty of cumulative CO_2 leakage and ensure an efficient risk management in the life-cycle of a GCS project.

4. The incremental reduction in uncertainty in the cumulative CO_2 leakage may not increase proportional to the distance from the injection well, and is a strong function of the reservoir permeability heterogeneity. Thus, an optimal monitoring well placement and measurement type is important to minimize present and future potential risks.

5. The subgrid for the possible monitoring well locations will have a major impact in the optimal monitoring design. The uncertainty reduction obtained at the monitoring locations will depend on the geologic heterogeneity, which affects the CO_2 plume movement in the subsurface. However, with proper knowledge of the geologic setting and a finer monitoring location subgrid, one can further optimize the monitoring design to further reduce the uncertainty in cumulative CO_2 leakage.

Future research in this topic includes investigating the effect of different monitoring measurement types, such as seismic sensing, or a combination of the available measurements. Similarly, multi-scale or local grid refinement to optimize the monitoring well placement can help improve the reduction in uncertainty for CO_2 leakage risks. Moreover, a global optimization strategy, such as genetic algorithm or simulated annealing, can provide more computationally efficient results for finer subgrids. Other alternatives could include incorporating other data assimilation techniques such as EnKF or ESMDA, or performing spatial data assimilation rather than assimilating point-wise measurements. Including other risks such as geomechanical failure can help characterize a GCS site and provide a more in-depth risk management program.

Declaration of Competing Interest

The authors declare that they have no competing interests.

Acknowledgement

This project was funded by the US DOE's Fossil Energy Office through the National Risk Assessment Partnership (NRAP) managed by the National Energy Technology Laboratory (NETL). Numerical simulations

were performed on Los Alamos National Laboratory clusters supported by the High Performance Computing Division.

References

[1] Bert Metz. Carbon dioxide capture and storage: special report of the intergovernmental panel on climate change, 2005.

[2] K. Michael, A. Golab, V. Shulakova, J. Ennis-King, G. Allinson, S. Sharma, and T. Aiken. Geological storage of co2 in saline aquifers—a review of the experience from existing storage operations. *International Journal of Greenhouse Gas Control*, 4(4):659–667, 2010. ISSN 1750-5836. doi: https://doi.org/10.1016/j.ijggc.2009.12.011.

[3] A. Kopp, P.J. Binning, K. Johannsen, R. Helmig, and H. Class. A contribution to risk analysis for leakage through abandoned wells in geological co2 storage. *Advances in Water Resources*, 33(8): 867–879, 2010. doi: 10.1016/j.advwatres.2010.05.001. cited By 47.

[4] A. Goodman, G. Bromhal, B. Strazisar, T. Rodosta, W.F. Guthrie, D. Allen, and G. Guthrie. Comparison of methods for geologic storage of carbon dioxide in saline formations. *International Journal of Greenhouse Gas Control*, 18:329–342, 2013. doi: 10.1016/j.ijggc.2013.07.016. cited By 48.

[5] N. Castelletto, P. Teatini, G. Gambolati, D. Bossie-Codreanu, O. Vincké, J.-M. Daniel, A. Battistelli, M. Marcolini, F. Donda, and V. Volpi. Multiphysics modeling of co2 sequestration in a faulted saline formation in italy. *Advances in Water Resources*, 62:570–587, 2013. doi: 10.1016/j.advwatres.2013.04.006. cited By 25.

[6] B. Li and S.M. Benson. Influence of small-scale heterogeneity on upward co2plume migration in storage aquifers. *Advances in Water Resources*, 83:389–404, 2015. doi: 10.1016/j.advwatres.2015.07.010. cited By 84.

[7] J.S. Levine, I. Fukai, D.J. Soeder, G. Bromhal, R.M. Dilmore, G.D. Guthrie, T. Rodosta, S. Sanguinito, S. Frailey, C. Gorecki, W. Peck, and A.L. Goodman. U.s. doe netl methodology for estimating the prospective co2 storage resource of shales at the national and regional scale. *International Journal of Greenhouse Gas Control*, 51:81–94, 2016. doi: 10.1016/j.ijggc.2016.04.028. cited By 81.

[8] Mai Bui, Claire S. Adjiman, André Bardow, Edward J. Anthony, Andy Boston, Solomon Brown, Paul S. Fennell, Sabine Fuss, Amparo Galindo, Leigh A. Hackett, Jason P. Hallett, Howard J. Herzog, George

Jackson, Jasmin Kemper, Samuel Krevor, Geoffrey C. Maitland, Michael Matuszewski, Ian S. Metcalfe, Camille Petit, Graeme Puxty, Jeffrey Reimer, David M. Reiner, Edward S. Rubin, Stuart A. Scott, Nilay Shah, Berend Smit, J. P. Martin Trusler, Paul Webley, Jennifer Wilcox, and Niall Mac Dowell. Carbon capture and storage (ccs): the way forward. *Energy Environ. Sci.*, 11:1062–1176, 2018. doi: 10.1039/C7EE02342A. URL http://dx.doi.org/10.1039/C7EE02342A.

[9] Energy 2020. European commission. In *A strategy for competitive, sustainable and secure energy*, 2010.

[10] United nations. Agreement, p. *United Nations Treaty Collect*, pages 1–27, 2015.

[11] Zhenxue Dai, Hari Viswanathan, Richard Middleton, Feng Pan, William Ampomah, Changbing Yang, Wei Jia, Ting Xiao, Si Yong Lee, Brian McPherson, Robert Balch, Reid Grigg, and Mark White. Co2 accounting and risk analysis for co2 sequestration at enhanced oil recovery sites. *Environmental Science and Technology*, 50(14):7546–7554, 7 2016. ISSN 15205851. doi: 10.1021/acs.est.6b01744.

[12] D.R. Harp, R. Pawar, J.W. Carey, and C.W. Gable. Reduced order models of transient co2 and brine leakage along abandoned wellbores from geologic carbon sequestration reservoirs. *International Journal of Greenhouse Gas Control*, 45:150–162, 2 2016. ISSN 1750-5836. doi: 10.1016/j.ijggc.2015.12.001. cited By 38.

[13] J. Song and D. Zhang. Comprehensive review of caprock-sealing mechanisms for geologic carbon sequestration. *Environ Sci Technol*, 47(1):9–22, 2012.

[14] W. Sifuentes, M.J. Blunt, and M.A. Giddins. Modeling co2 storage in aquifers: Assessing the key contributors to uncertainty. volume 1, pages 148–160, 2009. cited By 38.

[15] J.M. Nordbotten, B. Flemisch, S.E. Gasda, H.M. Nilsen, Y. Fan, G.E. Pickup, B. Wiese, M.A. Celia, H.K. Dahle, G.T. Eigestad, and K. Pruess. Uncertainties in practical simulation of co2 storage. *International Journal of Greenhouse Gas Control*, 9:234–242, 2012. doi: 10.1016/j.ijggc.2012.03.007. cited By 78.

[16] S.M. Benson and L. Myer. 2003.

[17] E. Keating, D. Bacon, S. Carroll, K. Mansoor, Y. Sun, L. Zheng, D. Harp, and Z. Dai. Applicability of aquifer impact models to support decisions at co2 sequestration sites. *International Journal of Greenhouse Gas Control*, 52:319–330, 2016. doi: 10.1016/j.ijggc.2016.07.001.

[18] J. Condor, D. Unatrakarn, M. Wilson, and K. Asghari. A comparative analysis of risk assessment methodologies for the geologic storage of carbon dioxide. volume 4, pages 4036–4043, 2011. doi: 10.1016/j.egypro.2011.02.345.

[19] L. De Lary, J.-C. Manceau, A. Loschetter, J. Rohmer, O. Bouc, I. Gravaud, C. Chiaberge, P. Willaume, and T. Yalamas. Quantitative risk assessment in the early stages of a co2 geological storage project: Implementation of a practical approach in an uncertain context. *Greenhouse Gases: Science and Technology*, 5(1):50–63, 2015. doi: 10.1002/ghg.1447.

[20] Q. Li and G. Liu. *Risk assessment of the geological storage of CO2: A review*. 2016. doi: 10.1007/978-3-319-27019-7_13. cited By 39.

[21] J.-P. Nicot, C.M. Oldenburg, J.E. Houseworth, and J.-W. Choi. Analysis of potential leakage pathways at the cranfield, ms, u.s.a., co2 sequestration site. *International Journal of Greenhouse Gas Control*, 18:388–400, 2013. doi: 10.1016/j.ijggc.2012.10.011. cited By 38.

[22] T. Onishi, M.C. Nguyen, J.W. Carey, B. Will, W. Zaluski, D.W. Bowen, B.C. Devault, A. Duguid, Q. Zhou, S.H. Fairweather, L.H. Spangler, and P.H. Stauffer. Potential co2 and brine leakage through wellbore pathways for geologic co2 sequestration using the national risk assessment partnership tools: Application to the big sky regional partnership. *International Journal of Greenhouse Gas Control*, 81: 44–65, 2019. doi: 10.1016/j.ijggc.2018.12.002. cited By 30.

[23] Z. Dai, P.H. Stauffer, J.W. Carey, R.S. Middleton, Z. Lu, J.F. Jacobs, K. Hnottavange-Telleen, and L.H. Spangler. Pre-site characterization risk analysis for commercial-scale carbon sequestration. *Environmental Science and Technology*, 48(7):3908–3915, 2014. doi: 10.1021/es405468p.

[24] Y. Zhang, P. Vouzis, and N.V. Sahinidis. Gpu simulations for risk assessment in co2 geologic sequestration. *Computers and Chemical Engineering*, 35(8):1631–1644, 2011. doi: 10.1016/j.compchemeng.2011.03.023. cited By 20.

[25] R.A. Chadwick, R. Arts, and O. Eiken. 4d seismic quantification of a growing co2 plume at sleipner, north sea. *Petroleum Geology Conference Proceedings*, 6(0):1385–1399, 2005. doi: 10.1144/0061385. cited By 188.

[26] R.J. Pawar, G.S. Bromhal, S. Chu, R.M. Dilmore, C.M. Oldenburg, P.H. Stauffer, Y. Zhang, and G.D. Guthrie. The national risk assessment partnership's integrated assessment model for carbon storage: A tool to support decision making amidst uncertainty. *International Journal of Greenhouse Gas Control*, 52:175–189, 2016. doi: 10.1016/j.ijggc.2016.06.015. cited By 59.

[27] Y.-M. Yang, M.J. Small, E.O. Ogretim, D.D. Gray, A.W. Wells, G.S. Bromhal, and B.R. Strazisar. A bayesian belief network (bbn) for combining evidence from multiple co2 leak detection technologies. *Greenhouse Gases: Science and Technology*, 2(3):185–199, 2012. doi: 10.1002/ghg.1284.

[28] B. Ren, S. Ren, L. Zhang, G. Chen, and H. Zhang. Monitoring on co2 migration in a tight oil reservoir during ccs-eor in jilin oilfield china. *Energy*, 98:108–121, 2016. doi: 10.1016/j.energy.2016.01.028.

[29] Z. Dai, E. Keating, D. Bacon, H. Viswanathan, P. Stauffer, A. Jordan, and R. Pawar. Probabilistic evaluation of shallow groundwater resources at a hypothetical carbon sequestration site. *Scientific Reports*, 4, 2014. doi: 10.1038/srep04006. cited By 1.

[30] C. Yang, S.D. Hovorka, R.H. Treviño, and J. Delgado-Alonso. Integrated framework for assessing impacts of co2 leakage on groundwater quality and monitoring-network efficiency: Case study at a co2 enhanced oil recovery site. *Environmental Science and Technology*, 49(14):8887–8898, 2015. doi: 10.1021/acs.est.5b01574.

[31] L. Zhang, B. Ren, H. Huang, Y. Li, S. Ren, G. Chen, and H. Zhang. Co2 eor and storage in jilin oilfield china: Monitoring program and preliminary results. *Journal of Petroleum Science and Engineering*, 125:1–12, 2015. doi: 10.1016/j.petrol.2014.11.005.

[32] A. Chadwick, R. Arts, O. Eiken, P. Williamson, and G. Williams. Geophysical monitoring of the co2 plume at sleipner, north sea. *Advances in the Geological Storage of Carbon Dioxide*, pages 303–314, 2006. cited By 69.

[33] D. Grana, S. Verma, J. Pafeng, X. Lang, H. Sharma, W. Wu, F. McLaughlin, E. Campbell, K. Ng, V. Alvarado, S. Mallick, and J. Kaszuba. A rock physics and seismic reservoir characterization study of the rock springs uplift, a carbon dioxide sequestration site in southwestern wyoming. *International Journal of Greenhouse Gas Control*, 63:296–309, 2017. doi: 10.1016/j.ijggc.2017.06.004. cited By 23.

[34] E. Keating, Z. Dai, D. Dempsey, and R. Pawar. Effective detection of co2 leakage: A comparison of groundwater sampling and pressure monitoring. volume 63, pages 4163–4171, 2014. doi: 10.1016/j.egypro.2014.11.448.

[35] Z. Wang and M.J. Small. A bayesian approach to co2 leakage detection at saline sequestration sites using pressure measurements. *International Journal of Greenhouse Gas Control*, 30:188–196, 2014. doi: 10.1016/j.ijggc.2014.09.011.

[36] N.A. Azzolina, M.J. Small, D.V. Nakles, and G.S. Bromhal. Effectiveness of subsurface pressure monitoring for brine leakage detection in an uncertain co2 sequestration system. *Stochastic Environmental Research and Risk Assessment*, 28(4):895–909, 2014. doi: 10.1007/s00477-013-0788-9.

[37] Y. Oruganti, A.K. Gupta, and S.L. Bryant. Analytical estimation of risk due to pressure buildup during co2. volume 4, pages 4140–4147, 2011. doi: 10.1016/j.egypro.2011.02.358. cited By 8.

[38] O. Senel and N. Chugunov. Co2 injection in a saline formation: Pre-injection reservoir modeling and uncertainty analysis for illinois basin decatur project. volume 37, pages 4598–4611, 2013. doi: 10.1016/j.egypro.2013.06.368. cited By 13.

[39] Wenyue Sun and Louis J. Durlofsky. Data-space approaches for uncertainty quantification of co2 plume location in geological carbon storage. *Advances in Water Resources*, 123:234–255, 1 2019. ISSN 03091708. doi: 10.1016/j.advwatres.2018.10.028. cited By 23.

[40] Hewei Tang, Pengcheng Fu, Honggeun Jo, Su Jiang, Christopher S. Sherman, François Hamon, Nicholas A. Azzolina, and Joseph P. Morris. Deep learning-accelerated 3d carbon storage reservoir pressure forecasting based on data assimilation using surface displacement from insar. *International Journal of Greenhouse Gas Control*, 120:103765, 10 2022. ISSN 1750-5836. doi: 10.1016/J.IJGGC.2022.103765.

[41] Zhiwei Ma, Yong Do Kim, Oleg Volkov, and Louis J. Durlofsky. Optimization of subsurface flow operations using a dynamic proxy strategy. *Mathematical Geosciences*, 54:1261–1287, 11 2022. ISSN 18748953. doi: 10.1007/S11004-022-10020-2/FIGURES/16.

[42] *Machine Learning-Based Optimization of Well Locations and WAG Parameters under Geologic Uncertainty*, volume Day 3 Mon, April 16, 2018 of *SPE Improved Oil Recovery Conference*, 04 2018. doi: 10.2118/190239-MS.

[43] J.J. Butler Jr., C.D. McElwee, and G.C. Bohling. Pumping tests in networks of multilevel sampling wells: Motivation and methodology. *Water Resources Research*, 35(11):3553 – 3560, 1999. doi: 10.1029/1999WR900231. Cited by: 92; All Open Access, Bronze Open Access, Green Open Access.

[44] M. Cardiff, W. Barrash, and P.K. Kitanidis. A field proof-of-concept of aquifer imaging using 3-d transient hydraulic tomography with modular, temporarily-emplaced equipment. *Water Resources Research*, 48(5), 2012. doi: 10.1029/2011WR011704. Cited by: 88; All Open Access, Bronze Open Access, Green Open Access.

[45] R. Brauchler, R. Hu, L. Hu, S. Jiménez, P. Bayer, P. Dietrich, and T. Ptak. Rapid field application of hydraulic tomography for resolving aquifer heterogeneity in unconsolidated sediments. *Water Resources Research*, 49(4):2013 – 2024, 2013. doi: 10.1002/wrcr.20181. Cited by: 53.

[46] Bailian Chen, Dylan R. Harp, Zhiming Lu, and Rajesh J. Pawar. Reducing uncertainty in geologic co2 sequestration risk assessment by assimilating monitoring data. *International Journal of Greenhouse Gas Control*, 94, 3 2020. ISSN 17505836. doi: 10.1016/j.ijggc.2019.102926.

[47] Alexander Y. Sun, Jean Philippe Nicot, and Xiaodong Zhang. Optimal design of pressure-based, leakage detection monitoring networks for geologic carbon sequestration repositories. *International Journal of Greenhouse Gas Control*, 19:251–261, 2013. ISSN 17505836. doi: 10.1016/j.ijggc.2013.09.005.

[48] C.J. Seto and G.J. McRae. Reducing risk in basin scale co2 sequestration: A framework for integrated monitoring design. *Environmental Science and Technology*, 45(3):845–859, 2011. doi: 10.1021/es102240w.

[49] Catherine M.R. Yonkofski, Jason A. Gastelum, Ellen A. Porter, Luke R. Rodriguez, Diana H. Bacon, and Christopher F. Brown. An optimization approach to design monitoring schemes for co2 leakage detection. *International Journal of Greenhouse Gas Control*, 47:233–239, 4 2016. ISSN 17505836. doi: 10.1016/j.ijggc.2016.01.040.

[50] Javier E. Santos, Bernard Chang, Alex Gigliotti, Eric Guiltinan, Mohamed Mehana, Arvind Mohan, James McClure, Qinjun Kang, Hari Viswanathan, Nicholas Lubbers, Masa Prodanovic, and Michael Pyrcz. Learning from a big dataset of digital rock simulations. In *AGU Fall Meeting Abstracts*, volume 2021, pages H25O–1207, December 2021.

[51] Zeeshan Tariq, Murtada Saleh Aljawad, Amjed Hasan, Mobeen Murtaza, Emad Mohammed, Ammar El-Husseiny, Sulaiman A Alarifi, Mohamed Mahmoud, and Abdulazeez Abdulraheem. A systematic review of data science and machine learning applications to the oil and gas industry. *Journal of Petroleum Exploration and Production Technology*, pages 1–36, 2021.

[52] Mohammad Ali Mirza, Mahtab Ghoroori, and Zhangxin Chen. Intelligent petroleum engineering. *Engineering*, 18:27–32, 2022. ISSN 2095-8099. doi: https://doi.org/10.1016/j.eng.2022.06.009.

[53] *Best Practices in Automatic Permeability Estimation: Machine-Learning Methods vs. Conventional Petrophysical Models*, volume Day 4 Tue, June 13, 2023 of *SPWLA Annual Logging Symposium*, 06 2023. doi: 10.30632/SPWLA-2023-0084.

[54] Wen Pan, Carlos Torres-Verdín, Ian Duncan, and Michael Pyrcz. Reducing the uncertainty of multi-well petrophysical interpretation from well logs via machine-learning and statistical models. 03 2022. doi: 10.31223/X5WP8D.

[55] E. Laloy, R. Hérault, D. Jacques, and N. Linde. Training-image based geostatistical inversion using a spatial generative adversarial neural network. *Water Resources Research*, 54(1):381–406, 2018. doi: 10.1002/2017WR022148. cited By 206.

[56] Y. Liu, W. Sun, and L.J. Durlofsky. A deep-learning-based geological parameterization for history matching complex models. *Mathematical Geosciences*, 51(6):725–766, 2019. doi: 10.1007/s11004-019-09794-9. cited By 66.

[57] C. Etienam. 4d seismic history matching incorporating unsupervised learning. 2019. doi: 10.2118/195500-ms. cited By 6.

[58] M. H Hassoun. *Fundamentals of artificial neural networks*. MIT press., 1995.

[59] B Yegnanarayana. *Artificial neural networks*. PHI Learning Pvt. Ltd., 2009.

[60] B. Yeten, A. Castellini, B. Guyaguler, and W.H. Chen. A comparison study on experimental design and response surface methodologies. *A Comparison Study on Experimental Design and Response Surface Methodologies*, 2005. cited By 20.

[61] B. Chen, J. He, X. Wen, W. Chen, and A. Reynolds. Pilot design analysis using proxies and markov chain monte carlo method. 2016. doi: 10.3997/2214-4609.201601821.

[62] M. Babaei and I. Pan. Performance comparison of several response surface surrogate models and ensemble methods for water injection optimization under uncertainty. *Computers and Geosciences*, 91:19–32, 2016. doi: 10.1016/j.cageo.2016.02.022. cited By 41.

[63] Z. Guo and A.C. Reynolds. Robust life-cycle production optimization with a support-vector-regression proxy. *SPE Journal*, 23(6):2409–2427, 2018. doi: 10.2118/191378-PA. cited By 88.

[64] W. Ampomah, R.S. Balch, M. Cather, R. Will, D. Gunda, Z. Dai, and M.R. Soltanian. Optimum design of co2 storage and oil recovery under geological uncertainty. *Applied Energy*, 195:80–92, 2017. doi: 10.1016/j.apenergy.2017.03.017. cited By 155.

[65] C. Wang, G. Li, and A.C. Reynolds. Production optimization in closed-loop reservoir management. *SPE Journal*, 14(3):506–523, 2009. doi: 10.2118/109805-PA. cited By 201.

[66] Proctor Joshua Brunton, Steve and Nathan Kutz. Discovering governing equations from data by sparse identification of nonlinear dynamical systems. *Proceedings of the National Academy of Sciences of the United States of America*, 2016. doi: 10.1073/pnas.1517384113.

[67] He Xiaolong Fries, William and Youngsoo Choi. Lasdi: Parametric latent space dynamics identification. *Computer Methods in Applied Mechanics and Engineering*, 2022. doi: 10.1016/j.cma.2022.115436.

[68] Choi Youngsoo Fries William Belof Jonathan He, Xiaolong and Jiun-Shyan Chen. glasdi: Parametric physics-informed greedy latent space dynamics identification. *Journal of Computational Physics*, 2023.

[69] David J. Lucia, Philip S. Beran, and Walter A. Silva. Reduced-order modeling: new approaches for computational physics. *Progress in Aerospace Sciences*, 40(1-2):51–117, 2 2004. ISSN 0376-0421. doi: 10.1016/J.PAEROSCI.2003.12.001.

[70] M. A. Cardoso, L. J. Durlofsky, and P. Sarma. Development and application of reduced-order modeling procedures for subsurface flow simulation. *International Journal for Numerical Methods in Engineering*, 77(9):1322–1350, 2 2009. ISSN 00295981. doi: 10.1002/nme.2453.

[71] Y. Zhu, N. Zabaras, P.-S. Koutsourelakis, and P. Perdikaris. Physics-constrained deep learning for high-dimensional surrogate modeling and uncertainty quantification without labeled data. *Journal of Computational Physics*, 394:56–81, 2019. doi: 10.1016/j.jcp.2019.05.024. cited By 393.

[72] Z.L. Jin, Y. Liu, and L.J. Durlofsky. Deep-learning-based surrogate model for reservoir simulation with time-varying well controls. *Journal of Petroleum Science and Engineering*, 192:107273, 9 2020. ISSN 0920-4105. doi: 10.1016/j.petrol.2020.107273. cited By 53.

[73] Gege Wen, Zongyi Li, Qirui Long, Kamyar Azizzadenesheli, Anima Anandkumar, and Sally M. Benson. Real-time high-resolution co 2 geological storage prediction using nested fourier neural operators. *Energy & Environmental Science*, 2023. ISSN 1754-5692. doi: 10.1039/d2ee04204e.

[74] Gege Wen, Catherine Hay, and Sally M. Benson. Ccsnet: A deep learning modeling suite for co2 storage. *Advances in Water Resources*, 155:104009, 9 2021. ISSN 0309-1708. doi: 10.1016/J.ADVWATRES.2021.104009.

[75] Eduardo Maldonado-Cruz and Michael J. Pyrcz. Fast evaluation of pressure and saturation predictions with a deep learning surrogate flow model. *Journal of Petroleum Science and Engineering*, 212:110244, 5 2022. ISSN 0920-4105. doi: 10.1016/J.PETROL.2022.110244.

[76] Syamil Mohd Razak, Anyue Jiang, and · Behnam Jafarpour. Latent-space inversion (lsi): a deep learning framework for inverse mapping of subsurface flow data. *Computational Geoscience*, 26:71–99, 11 2022. doi: 10.1007/s10596-021-10104-8.

[77] Yong Do Kim and Louis J. Durlofsky. Convolutional – recurrent neural network proxy for robust optimization and closed-loop reservoir management. *Computational Geosciences*, pages 1–24, 1 2023. ISSN 1420-0597. doi: 10.1007/S10596-022-10189-9/TABLES/1.

[78] Y. Zhu and N. Zabaras. Bayesian deep convolutional encoder–decoder networks for surrogate modeling and uncertainty quantification. *Journal of Computational Physics*, 366:415–447, 2018. doi: 10.1016/j.jcp.2018.04.018. cited By 313.

[79] N. Wang, H. Chang, and D. Zhang. Efficient uncertainty quantification for dynamic subsurface flow with surrogate by theory-guided neural network. *Computer Methods in Applied Mechanics and Engineering*, 373, 2021. doi: 10.1016/j.cma.2020.113492. cited By 33.

[80] L. Mohamed, M. Christie, and V. Demyanov. Comparison of stochastic sampling algorithms for uncertainty quantification. *SPE Journal*, 15(1):31–38, 2010. doi: 10.2118/119139-PA. cited By 107.

[81] B. Chen, J. He, X.-H. Wen, W. Chen, and A.C. Reynolds. Uncertainty quantification and value of information assessment using proxies and markov chain monte carlo method for a pilot project. *Journal of Petroleum Science and Engineering*, 157:328–339, 2017. doi: 10.1016/j.petrol.2017.07.039.

[82] M.A. Cremon, M.A. Christie, and M.G. Gerritsen. Monte carlo simulation for uncertainty quantification in reservoir simulation: A convergence study. *Journal of Petroleum Science and Engineering*, 190, 2020. doi: 10.1016/j.petrol.2020.107094. cited By 11.

[83] G. Bellenfant, D. Guyonnet, D. Dubois, and O. Bouc. Uncertainty theories applied to the analysis of co2 plume extension during geological storage. volume 1, pages 2447–2454, 2009. doi: 10.1016/j.egypro.2009.02.006. cited By 8.

[84] S. Li, Y. Zhang, and X. Zhang. A study of conceptual model uncertainty in large-scale co2 storage simulation. *Water Resources Research*, 47(5), 2011. doi: 10.1029/2010WR009707. cited By 24.

[85] W. Jia, B. McPherson, F. Pan, Z. Dai, and T. Xiao. Uncertainty quantification of co2 storage using bayesian model averaging and polynomial chaos expansion. *International Journal of Greenhouse Gas Control*, 71:104–115, 2018. doi: 10.1016/j.ijggc.2018.02.015. cited By 23.

[86] H. Jeong, S. Srinivasan, and S. Bryant. Uncertainty quantification of co2 plume migration using static connectivity of geologic features. volume 37, pages 3771–3779, 2013. doi: 10.1016/j.egypro.2013.06.273. cited By 8.

[87] R.S. Jayne, H. Wu, and R.M. Pollyea. Geologic co2 sequestration and permeability uncertainty in a highly heterogeneous reservoir. *International Journal of Greenhouse Gas Control*, 83:128–139, 2019. doi: 10.1016/j.ijggc.2019.02.001. cited By 29.

[88] A.A. Emerick and A.C. Reynolds. Combining the ensemble kalman filter with markov chain monte carlo for improved history matching and uncertainty characterization. *SPE Journal*, 17(2):418–440, 2012. doi: 10.2118/141336-PA.

[89] N. Liu and D.S. Oliver. Evaluation of monte carlo methods for assessing uncertainty. *SPE Journal*, 8 (2):188–195, 2003. doi: 10.2118/84936-PA.

[90] Y. Chen and D.S. Oliver. Ensemble randomized maximum likelihood method as an iterative ensemble smoother. *Mathematical Geosciences*, 44(1):1–26, 2012. doi: 10.1007/s11004-011-9376-z. cited By 249.

[91] Eric Bhark and Kaveh Dehghani. Assisted history matching benchmarking: Design of experiments-based techniques. In *SPE Annual Technical Conference and Exhibition*. OnePetro, 2014.

[92] Hyucksoo Park, Céline Scheidt, Darryl Fenwick, Alexandre Boucher, and Jef Caers. History matching and uncertainty quantification of facies models with multiple geological interpretations. *Computational Geosciences*, 17:609–621, 2013.

[93] Xianlin Ma, Mishal Al-Harbi, Akhil Datta-Gupta, and Yalchin Efendiev. An efficient two-stage sampling method for uncertainty quantification in history matching geological models. *SPE Journal*, 13 (01):77–87, 2008.

[94] J. Caers. *Modeling Uncertainty in the Earth Sciences*. 2011. doi: 10.1002/9781119995920.

[95] Y. Chen and D.S. Oliver. Cross-covariances and localization for enkf in multiphase flow data assimilation. *Computational Geosciences*, 14(4):579–601, 2010. doi: 10.1007/s10596-009-9174-6.

[96] H. Chang, D. Zhang, and Z. Lu. History matching of facies distribution with the enkf and level set parameterization. *Journal of Computational Physics*, 229(20):8011–8030, 2010. doi: 10.1016/j.jcp.2010.07.005.

[97] Reza Tavakoli, Hongkyu Yoon, Mojdeh Delshad, Ahmed H ElSheikh, Mary F Wheeler, and Bill W Arnold. Comparison of ensemble filtering algorithms and null-space monte carlo for parameter estimation and uncertainty quantification using co2 sequestration data. *Water Resources Research*, 49(12): 8108–8127, 2013.

[98] Ismael Dawuda and Sanjay Srinivasan. Geologic modeling and ensemble-based history matching for evaluating co2 sequestration potential in point bar reservoirs. *Frontiers in Energy Research*, 10:867083, 2022.

[99] W. Ma, B. Jafarpour, and J. Qin. Dynamic characterization of geologic co2 storage aquifers from monitoring data with ensemble kalman filter. *International Journal of Greenhouse Gas Control*, 81: 199–215, 2019. doi: 10.1016/j.ijggc.2018.10.009. cited By 14.

[100] J. Rafiee and A.C. Reynolds. Theoretical and efficient practical procedures for the generation of inflation factors for es-mda. *Inverse Problems*, 33(11), 2017. doi: 10.1088/1361-6420/aa8cb2. cited By 38.

[101] Atefeh Jahandideh, Siavash Hakim-Elahi, and Behnam Jafarpour. Inference of rock flow and mechanical properties from injection-induced microseismic events during geologic co2 storage. *International Journal of Greenhouse Gas Control*, 105:103206, 2021.

[102] Amine Tadjer and Reidar B Bratvold. Managing uncertainty in geological co2 storage using bayesian evidential learning. *Energies*, 14(6):1557, 2021.

[103] Su Jiang and Louis J Durlofsky. Data-space inversion using a recurrent autoencoder for time-series parameterization. *Computational Geosciences*, 25:411–432, 2021.

[104] Yimin Liu and Louis J Durlofsky. 3d cnn-pca: A deep-learning-based parameterization for complex geomodels. *Computers & Geosciences*, 148:104676, 2021.

[105] Siddharth Misra, Yusuf Falola, Polina Churilova, Rui Liu, Chung-Kan Huang, and Jose F Delgado. Deep learning assisted extremely low-dimensional representation of subsurface earth. *Available at SSRN 4196705*, 2022.

[106] S. Oladyshkin, H. Class, and W. Nowak. Bayesian updating via bootstrap filtering combined with data-driven polynomial chaos expansions: Methodology and application to history matching for carbon dioxide storage in geological formations. *Computational Geosciences*, 17(4):671–687, 2013. doi: 10.1007/s10596-013-9350-6. cited By 36.

[107] Mingliang Liu and Dario Grana. Petrophysical characterization of deep saline aquifers for co2 storage using ensemble smoother and deep convolutional autoencoder. *Advances in Water Resources*, 142, 8 2020. ISSN 03091708. doi: 10.1016/j.advwatres.2020.103634.

[108] Mohamed Mehana, Bailian Chen, and Rajesh Pawar. Reduced-order models for wellbore leakage from depleted reservoirs. Unconventional Resources Technology Conference (URTEC), 2022. doi: 10.15530/urtec-2022-3725868.

[109] Rajesh Pawar, Shaoping Chu, Bill Carey, David Tu, Nathan Moodie, Bailian Chen, and William Ampomah. Quantitative risk assessment of leakage through legacy wells in support of permit application for a large-scale co 2 injection project in southwestern us, 2022.

[110] Bailian Chen, Dylan R. Harp, Youzuo Lin, Elizabeth H. Keating, and Rajesh J. Pawar. Geologic co2 sequestration monitoring design: A machine learning and uncertainty quantification based approach. *Applied Energy*, 225:332–345, 9 2018. ISSN 03062619. doi: 10.1016/j.apenergy.2018.05.044.

[111] J.H. Friedman. Multivariate adaptive regression splines. *Annals of Statistics*, 19(1):1–141, 1991.

[112] D.H. Le and A.C. Reynolds. Optimal choice of a surveillance operation using information theory. *Computational Geosciences*, 18(3-4):505–518, 2014. doi: 10.1007/s10596-014-9401-7.

[113] R.L. Iman. Latin hypercube sampling. *Latin Hypercube Sampling*, 2008.

[114] J. C. Helton and F. J. Davis. Latin hypercube sampling and the propagation of uncertainty in analyses of complex systems. *Reliability Engineering & System Safety*, 81(1):23–69, 7 2003. ISSN 0951-8320. doi: 10.1016/S0951-8320(03)00058-9.

[115] G.A. Zyvoloski, B.A. Robinson, Z.V. Dash, and L.L. Trease. Summary of the models and methods for the fehm application - a finite-element heat- and mass-transfer code. *Rep. LA-13307-MS*, 1997. cited By 165.

[116] Y. Xu and R. Goodacre. On splitting training and validation set: A comparative study of cross-validation, bootstrap and systematic sampling for estimating the generalization performance of supervised learning. *Journal of Analysis and Testing*, 2(3):249–262, 2018. cited By 311.

[117] Martín Abadi, Ashish Agarwal, Paul Barham, Eugene Brevdo, Zhifeng Chen, Craig Citro, Greg S. Corrado, Andy Davis, Jeffrey Dean, Matthieu Devin, Sanjay Ghemawat, Ian Goodfellow, Andrew Harp, Geoffrey Irving, Michael Isard, Yangqing Jia, Rafal Jozefowicz, Lukasz Kaiser, Manjunath Kudlur, Josh Levenberg, Dandelion Mané, Rajat Monga, Sherry Moore, Derek Murray, Chris Olah, Mike Schuster, Jonathon Shlens, Benoit Steiner, Ilya Sutskever, Kunal Talwar, Paul Tucker, Vincent Vanhoucke, Vijay Vasudevan, Fernanda Viégas, Oriol Vinyals, Pete Warden, Martin Wattenberg, Martin Wicke, Yuan Yu, and Xiaoqiang Zheng. Tensorflow: Large-scale machine learning on heterogeneous systems, 2015. Software available from tensorflow.org.

[118] François Chollet et al. Keras. https://keras.io, 2015.

[119] Diederik Kingma and Jimmy Ba. Adam: A method for stochastic optimization. *International Conference on Learning Representations*, 12 2014.

[120] J. Caers. *Petroleum Geostatistics*, 2005. cited By 186.

[121] B. Chen and A.C. Reynolds. Optimal control of icv's and well operating conditions for the water-alternating-gas injection process. *Journal of Petroleum Science and Engineering*, 149:623–640, 2017. doi: 10.1016/j.petrol.2016.11.004.

[122] D. George, A. Kuprat, N. Carlson, and C. Gable. *LaGriT - Los Alamos Grid Toolbox*, 1999. cited By 6.

[123] S. Geisser. *Predictive Inference: An Introduction*, 1993.

[124] Diana Koschel, Jean-Yves Coxam, Laurence Rodier, and Vladimir Majer. Enthalpy and solubility data of co2 in water and nacl (aq) at conditions of interest for geological sequestration. *Fluid phase equilibria*, 247(1-2):107–120, 2006.

[125] G. Evensen. *Data assimilation: The ensemble kalman filter*. 2009. doi: 10.1007/978-3-642-03711-5. cited By 1238.

[126] A.A. Emerick and A.C. Reynolds. Ensemble smoother with multiple data assimilation. *Computers and Geosciences*, 55:3–15, 2013. doi: 10.1016/j.cageo.2012.03.011. cited By 618.